Accessing the Dynamics of End-Grafted Flexible Polymer Chains by Atomic Force-Electrochemical Microscopy. Theoretical Modeling of the Approach Curves by the Elastic Bounded Diffusion Model and Monte Carlo Simulations. Evidence for Compression-Induced Lateral Chain Escape

Jeremy Abbou, Agnès Anne, and Christophe Demaille*

Laboratoire d'Electrochimie Moléculaire, Unité Mixte de Recherche Université−CNRS No. 7591, Université de Paris 7−Denis Diderot, 2 place Jussieu, 75251 Paris Cedex 05, France

Received: July 19, 2006; In Final Form: September 12, 2006

The dynamics of a molecular layer of linear poly(ethylene glycol) (PEG) chains of molecular weight 3400, bearing at one end a ferrocene (Fc) label and thiol end-grafted at a low surface coverage onto a gold substrate, is probed using combined atomic force−electrochemical microscopy (AFM-SECM), at the scale of ∼100 molecules. Force and current approach curves are simultaneously recorded as a force-sensing microelectrode (tip) is inserted within the ∼10 nm thick, redox labeled, PEG chain layer. Whereas the force approach curve gives access to the structure of the compressed PEG layer, the tip-current, resulting from tip-to-substrate redox cycling of the Fc head of the chain, is controlled by chain dynamics. The elastic bounded diffusion model, which considers the motion of the Fc head as diffusion in a conformational field, complemented by Monte Carlo (MC) simulations, from which the chain conformation can be derived for any degree of confinement, allows the theoretical tip-current approach curve to be calculated. The experimental current approach curve can then be very satisfyingly reproduced by theory, down to a tip−substrate separation of ∼2 nm, using only one adjustable parameter characterizing the chain dynamics: the effective diffusion coefficient of the chain head. At closer tip−substrate separations, an unpredicted peak is observed in the experimental current approach curve, which is shown to find its origin in a compression-induced escape of the chain from within the narrowing tip−substrate gap. MC simulations provide quantitative support for lateral chain elongation as the escape mechanism.

Introduction

Determining the dynamics of linear flexible polymeric chains is a topic of current interest, whether these molecules are synthetic polymers[1] or biomolecules such as DNA[2] or peptide chains.[3] Most of the reported works in this field are concerned with the dynamics of free chains *in solution* and often consist of cyclization rate experiments[2a−d] or in transient spectroscopic studies of energy transfer between fluorescent markers labeling each extremity of the chains.[2e−f,3] However, very few experimental techniques exist to characterize the dynamics of linear chains *end-grafted* to surfaces,[4] even though such systems are highly relevant for numerous biotechnical and biomedical applications such as biosensors, drug delivery devices, membranes, and engineered nanostructures.

In this context, we recently introduced the use of atomic force−electrochemical microscopy (AFM-SECM),[5] an electrochemical near-field in situ technique combining atomic force[6] and electrochemical microscopy,[7] to quantitatively probe both the conformation and dynamics of nanometer-sized, end-grafted polymer chains.[8] The experimental system consisted of a molecular layer of linear flexible poly(ethylene glycol) (PEG) chains of molecular weight 3400, bearing at one end a ferrocene (Fc) head and covalently thiol-attached by their other extremity to a gold substrate. When, in an aqueous solution, a nanometer-sized spherical microelectrode-tip, mounted as a combined AFM-SECM probe, and biased at a positive enough potential, was approached from the gold substrate, the ferrocene heads borne by the substrate-tethered PEG chains were oxidized into ferrocenium (Fc^+) at the microelectrode and subsequently reduced back to their ferrocene state by the appropriately biased substrate. The Faradaic current circulating through the tip, resulting from the tip-to-substrate cycling of the ferrocene heads, was shown to be controlled by the chain flexibility and therefore to directly reflect the dynamics of the chain motion. The tip-current response was analyzed quantitatively, making use of the phenomenological model of elastic bounded diffusion that we introduced previously,[9a] according to which the chain is assimilated to an harmonic spring. Variation of the chain dynamics with increasing chain surface coverage was also analyzed.

We show here that, in the case of low surface coverage, where the chains are sufficiently far apart not to interact (the so-called mushroom regime),[10] modeling of the system dynamics can be greatly refined by the use of Monte Carlo (MC) simulations that allow the theoretical conformation of individual end-grafted polymer chains to be determined. In particular, the exact distribution of the ferrocene head in the tip−substrate gap, and its dependence upon chain compression, can be derived. MC simulations are also used to gain some insights into the occurrence of a peak in the current approach curve at close tip−substrate separations, an unexpected phenomenon we observed previously[8] but did not discuss in detail.

* Corresponding author. E-mail: demaille@paris7.jussieu.fr.

10.1021/jp064559i CCC: $33.50
Published on Web 10/24/2006

Experimental Methods

PEG_{3400} Derivatives and Materials. The PEG molecule NHS-PEG_{3400}-Fc (~79 monomer units), bearing an *N*-hydroxysuccinimide (NHS) activated ester at one end and a ferrocenyl (Fc) redox label at the other end, was synthesized as described elsewhere.[11]

2-Aminoethanethiol (cysteamine, >98%) and sodium perchlorate ($NaClO_4$) monohydrate were purchased from Fluka and Merck, respectively. Other commercial chemicals were reagent grade or better quality and used as received. All aqueous solutions were made with Milli-Q purified water (Millipore). All solvents used for PEG-grafting of gold substrate surfaces as well as AFM-SECM experiments were filtered before use on a 0.22 μm nylon Cameo filter.

Preparation of the Template-Stripped Gold Substrate Surface. The smooth template-stripped gold on mica substrates were prepared following a procedure adapted from the literature.[12] The gold surface was separated from the mica just before use by soaking the sandwich in THF for 2 min and then pulling the mica from the flat gold surface bearing glass slide. The gold surface was then rinsed successively with ethanol and Milli-Q water. Contact-mode AFM characterization of the freshly stripped surface was carried out using conventional AFM probes. Only the surfaces having an average roughness of less than 1 nm were immediately thiolated with cysteamine. When required, the evaluation of the effective area of the gold substrates was carried out as previously reported[13] by integration of the reduction peak of the gold oxide monolayer formed by cycling the substrate in a 0.5 M H_2SO_4 solution.[14] We reproducibly found an effective substrate surface area of 2.5 cm^2 (corresponding to a roughness of ~2), and we thus used this value to calculate the chain surface coverage.

Preparation of End-Grafted PEG Monolayers on Gold Substrate Surfaces. The liquid cell in which the gold substrate surface was mounted was filled with a 5 mM cysteamine solution in ethanol (filtered through a 0.05 μm Isopore Millipore membrane) and kept for 2 h under a nitrogen atmosphere, after which the surface was thoroughly rinsed with ethanol and Milli-Q water. A Fc-PEG_{3400}-NHS solution in phosphate buffer pH 7 was then introduced into the liquid cell and left to react with the cysteamine-derivatized surface. The final chain-grafting coverage was adjusted to be around $\sim 5 \times 10^{-12}$ mol/cm^2 by choosing a low Fc-PEG_{3400}-NHS solution concentration of 0.5 mM and a short reaction time of 3 min. Prior to the AFM-SECM experiment, the surface was thoroughly rinsed with Milli-Q water.

Fabrication and Characteristics of the Combined AFM-SECM Probes (Tips). The combined AFM-SECM probes bearing submicrometer-sized spherical electrode tips were fabricated as previously reported.[15] Briefly, a ~5 mm long 60 μm diameter gold wire was bent to a right angle ~1 mm away from one of its ends, while its other end was flattened between stainless steel plates. The short extremity of the wire was then etched electrochemically and its very end thus given a roughly conical shape. A spark discharge of controlled intensity was then used to locally fuse the very end of the wire that rounded up instantaneously upon cooling. In the present work, the spark generator was set to generate exclusively spherical tips having a diameter around ~0.5 μm. The surface of the spherical tip end was previously shown by scanning electron microscopy imaging to be extremely smooth. The probe was then entirely insulated by deposition of electrophoretic paint and was glued onto a standard AFM silicon chip. Shortly before use, a high-voltage pulse was applied to the probe to selectively expose its spherical tip end. To remove any residual contaminant, the tip was finally electrochemically cleaned by immersing its very end in a 0.5 M H_2SO_4 solution while scanning its potential between +0.3 and +1.8 V/SCE at 2 V/s for about 10 cycles. The exact value of the spherical tip radius was determined by scanning electron microscopy. Complete characterization of the electrochemical behavior of the combined AFM-SECM probes was carried out as reported elsewhere.[15]

Calculation of the Spring Constant of the Combined Probes. The spring constant of the combined probe, k_{probe}, was estimated from the measured dimensions of the flattened part of the wire-based probe that acted as a rectangular cantilever, using the formula:[16] $k_{probe} = Ewt^3/4l^3$, where w, t, and l stand respectively for the cantilever width, thickness, and length, and E is the elastic modulus of gold (~80 Gpa).[17]

AFM-SECM Experiments. The AFM/SECM experiments were performed with a Molecular Imaging PICOSPM AFM microscope (Scientec, France), which was modified and operated as previously described. Experiments were carried out in situ in a fluid cell containing an aq 1 M $NaClO_4$ electrolyte solution. A homemade bipotentiostat enabled the tip and substrate potentials to be independently controlled with respect to a quasireference electrode (an AgCl coated silver wire). The counter electrode was a platinum wire. The quasireference electrode was calibrated against a KCl-saturated calomel electrode (SCE). The tip and substrate currents were measured by the high (100 pA/V) and low (20 μA/V) gain current measuring circuits of the bipotentiostat. The tip biasing circuit was kept opened when the tip was at rest onto the surface, that is, when the AFM-force feedback loop was *on*. As a result, no long-lasting tip−substrate short circuit could occur. For each experiment, 5−10 AFM-SECM approach curves were acquired at different locations on the substrate. To avoid tip contamination, the tip was systematically withdrawn from the surface, cycled in situ between −0.3 and +1.2 V vs Ag/AgCl QRE at 0.5 V/s and moved over the substrate to a new location before acquisition of each approach curve. During the measurements, the microscope head was placed inside a homemade vibration-proof Faraday cage.

Monte Carlo Simulations: Simulation of the Chain Conformation by Self-Avoiding-Random Walks (SAW). Chain conformations were generated randomly by disposing the successive monomers of the chain on a cubic lattice, following a three-dimensional self-avoiding walk (SAW) starting at the chain anchoring point.[18] The position of each new monomer was chosen randomly from the *available* possible positions, i.e., the positions not occupied by either the substrate, the tip, or a previously placed monomer. As a result, the generated conformations do not occur with equal probability, and every configuration has to be weighted by a proper statistical weight following the Rosenbluth and Rosenbluth algorithm.[19] This method has been shown to satisfyingly reproduce the conformation of both end-grafted[20] and confined[21] polymeric chains. The results of the Monte Carlo−SAW simulations ran here were validated by comparing the dependence of the grafted chain dimensions ($\langle X \rangle$, R_F) on the chain length (N) with both the reported values for finite-length chains and with the asymptotic trends predicted for infinitely long chains (see Supporting Information). Typically 10^5−10^6 conformations were generated and sampled at each run.

Results and Discussion

Cyclic Voltammetry of a Gold Substrate Bearing the End-Grafted Fc-PEG Layer. Measurement of the PEG Chains Surface Coverage. A flat, template-stripped gold surface was

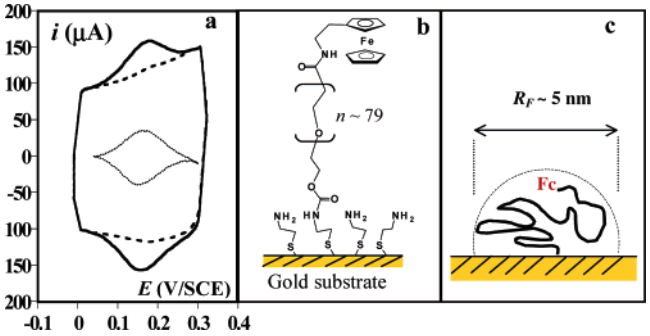

Figure 1. (a) Cyclic voltammogram at the gold substrate electrode. Solid line: Cyclic voltamogram of the Fc-PEG_{3400} bearing substrate. Dashed line: background signal recorded after the Fc-PEG layer had been electrochemically stripped. Dotted line: background corrected signal. Fc-PEG surface coverage $\Gamma = 0.5 \times 10^{-11}$ mol/cm^2. Scan rate $\upsilon = 5$ V/s. Supporting electrolyte 1 M $NaClO_4$. Effective surface area 2.5 cm^2. (b) Chemical representation of the grafted redox monolayer. (c) Depiction of a single Fc-PEG chain end grafted in a mushroom conformation. The dashed line represents the hemispherical volume statistically occupied by the chain.

first thiolated with cysteamine, and the NH_2 surface functionalities thus introduced were subsequently reacted with NHS-terminated PEG_{3400} chains bearing at their other extremity a redox-active alkyl-ferrocene (Fc), leading to the covalently derivatized substrate surface schematized in Figure 1.

The ferrocene heads borne by the chains were electrochemically detected by cyclic voltametry at the derivatized substrate immersed in an aqueous solution containing 1M $NaClO_4$ as a supporting electrolyte. As illustrated in Figure 1, characteristic Nersntian surface signals[22] were obtained: the separation between the peak potentials of the anodic and cathodic waves was small, <20 mV at 5 V/s, and the peak currents of the waves were proportional to the scan rate, while the current coincided with the background current at potentials much larger or much smaller than the peak potentials (see Figure 1a). Such a voltammetric behavior ensures that all the ferrocene heads are given ample time to reach the substrate and to reversibly exchange an electron with it. A value of $E° = 150 \pm 10$ mV/SCE was determined for the surface standard potential of the PEG-borne Fc/Fc^+ redox couple from the average value of the anodic and cathodic peak potentials; this latter value is in agreement with earlier reported values.[9,13] Integration of the current signal gave access to Γ, the surface coverage of grafted PEG-chains, each PEG chain bearing only one Fc head. Knowledge of the surface coverage is of particular importance for the present system because the structure of molecular layers formed by terminally attached linear polymeric chains is controlled by the chain surface coverage.[10] At coverage low enough for the chains not to overlap, the chain conformation is solely conditioned by the random walk of its monomers away from its anchoring point on the surface, and thus the grafted chains can be statistically viewed as hemispherical blobs (referred to as "mushrooms") of a size similar to their free Flory radius in solution, R_F (Figure 1c). In a good solvent, such as water for PEG, the Flory radius of the chains in solution is given by $R_F = aN^{3/5}$, N being the number of monomers of the chain and a the statistical monomer size.[23] In the present case, $N \sim 80$, thus, by taking $a = 0.35$ nm,[9b,24] we have $R_F \sim 5$ nm. The grafted chains can be considered as noninteracting when the average distance between the grafting point of the chains is larger than R_F,[10b] which translates here into an upper limit for the chain coverage of $\Gamma \sim 0.7 \times 10^{-11}$ mol/cm^2. By adjusting the grafting reaction conditions, PEG layers exhibiting a surface coverage of $\sim 0.5 \times 10^{-11}$ mol/cm^2 could be selectively prepared

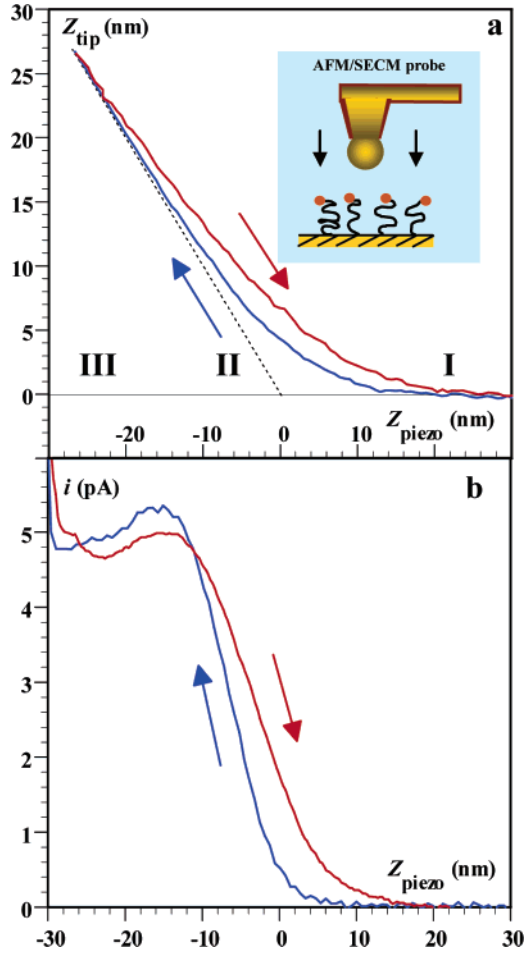

Figure 2. (a) Approach (blue) and retraction (red) deflection curves recorded during the approach of a combined AFM-SECM tip from the gold surface bearing end-grafted Fc-PEG chains. The tip deflection Z_{tip} is plotted as a function of Z_{piezo}, the elongation of the piezotube supporting the tip. (b) Simultaneously recorded current approach and retraction curves. In zone I, the tip is too far away from the surface to interact with the Fc-PEG layer. In zone II, the tip is compressing the layer. In zone III, the tip has made hard contact with the underlying substrate surface. The approach curves are recorded in situ in an aqueous solution containing $NaClO_4$ 1 M as the supporting electrolyte. The tip and surface are respectively biased at potentials of +0.4 V and −0.1 V vs SCE.

for AFM-SECM characterization (see Experimental Methods). This ensured that the grafted chains were in a mushroom configuration and that lateral interactions between neighboring chains could be neglected in the quantitative analysis of the AFM-SECM response of the system.

Tip Deflection and Tip Current Approach Curves of the End-Grafted PEG Layers in a 1 M $NaClO_4$ Aqueous Solution. In a typical experiment, a combined microelectrode probe (tip), biased at a potential positive enough with respect to the standard potential of the ferrocene head was approached, in a 1 M $NaClO_4$ aq solution (that is, with no electroactive species in the bulk solution), from a surface bearing Fc-PEG chains, biased negatively with respect to the standard potential of the Fc heads. The tip displacement away from its resting position, Z_{tip}, and the tip current i were simultaneously acquired and plotted as a function of the imposed piezoelongation Z_{piezo}. The resulting deflection and current approach curves (blue curves in Figure 2) can be delineated into three zones, as shown in Figure 2a: In zone I, the tip is far away from the surface, and neither deflection nor current is detected. In zone II, the tip starts to compress the polymer layer, which deforms under

load, and the cantilever arm supporting the tip bends upward. Concomitantly, a current begins to flow through the tip and increases while the tip is further pressed against the polymer layer until a broad current peak is reached. Further compression of the Fc-PEG layer results in a slight decrease followed by a sudden jump of the current as zone III was reached; this current jump is attributed to tunneling. At the same time, the tip motion vs piezoelongation plot becomes linear, indicating that the tip has made hard contact with the substrate (dashed line in Figure 2a). Importantly, when the tip is then pulled away from the surface, the then-recorded retraction curves (red curves in Figure 2) are similar to the approach curves, the observed offset being due to the piezohysteresis. It is also noteworthy that varying the tip approach speed from 10 to 50 nm/s had no effect on the approach curves, which supports the fact that the recorded curves were time independent.

The tip-to-substrate distance d, which is the distance of interest here, can be calculated from the value of the piezo elongation, Z_{piezo}, and of the tip deflection, Z_{tip}, by $d = Z_{piezo} + Z_{tip}$. Knowing the spring constant of the AFM-SECM combined probe (see Experimental Methods), the tip deflection was converted into a force (F) scale, and the force and current approach curves were plotted as a function of d, yielding typical combined AFM-SECM approach curves such as the ones presented in Figure 3, parts a and b.

We previously showed that the current approach curve recorded here is due to the Fc heads being electrochemically addressed by the microelectrode probe,[8] the Fc heads begin alternatively oxidized at the microelectrode and subsequently reduced at the substrate, as sketched in the inset of Figure 3b. The back and forth movement of the Fc heads shuttles the electrons from the substrate to the tip, thus giving rise to the tip current in a SECM positive feedback process.[7]

Because the tip and substrate potentials are respectively positive and negative enough with respect to the ferrocene head standard potential, the electron transfer steps are infinitely fast and the intensity of the feedback current is then kinetically controlled by the flexibility of the PEG chains. Quantitative analysis of the positive feedback response can thus give access to the dynamics of the PEG chains within the layer provided that an appropriate model is developed.

Quantitative Characterization of the SECM Eelectrochemical Approach Curves: Elastic Bounded Diffusion SECM Positive Feedback. Such a theoretical modeling can be carried out by making use of the elastic bounded diffusion model[9a] we introduced previously and adapted here as follows. We first consider that the chains are sandwiched between the anchoring plane and a planar tip located at an altitude d above it (see Figure 4a). The AFM-SECM experiments reported here specifically address the motion of the Fc head perpendicular to the substrate so that we will restrict the formulation of the analysis of the system dynamics to this sole dimension, denoted X (Figure 4a). Within the framework of the model, the chain is viewed as a simple springlike tether that elastically *opposes the motion of its Fc head* and is thus characterized by a spring constant k_{spr} and a chain head equilibrium position x_e. The Fc head then experiences an elastic force $F_{spr} = -k_{spr}(x - x_e)$ but also an osmotic force, resulting from the Fc head concentration gradient, expressed as $F_{os} = -(k_BT/C_p)(\partial C_p/\partial x)$, with k_B the Boltzmann constant and C_p the ferrocene head volume concentration in the gap at any x and time t. When the Fc head is in motion, a drag force $F_{dr} = -k_{dr}V$ must be overcome, with k_{dr} the corresponding drag coefficient and V the velocity of the Fc head. At the time scale of molecular motion, the ferrocene head

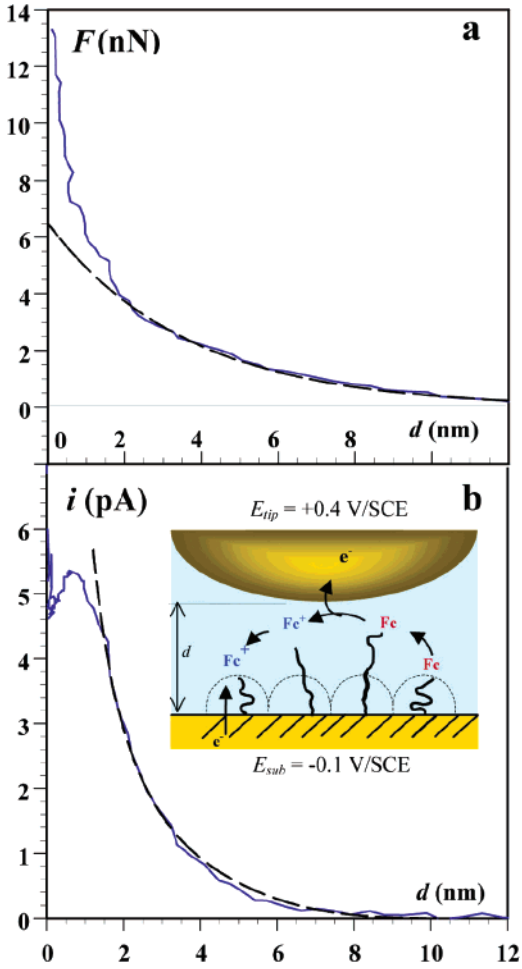

Figure 3. Deflection and current approach curves presented in Figure 2 replotted as a function of d, the tip−substrate separation derived as described in the text. (a) Force approach curve. The force exerted by the tip on the Fc-PEG layer, F, is calculated from the tip deflection, using the measured spring constant of the tip (see text), and plotted as a function of d (continuous line). The dashed line is the best-fit theoretical force curve for the compression of a layer of polymer chains in a mushroom configuration calculated using an apparent chain size of $R_{chain} = 4$ nm as the only adjustable parameter. (b) Simultaneously recorded current approach curve. The experimental approach curve (continuous line) is fitted by the theoretical elastic bounded positive feedback curve given by eq 5 (dashed curve) using, as a single adjustable parameter, the value of the characteristic current of $i_0 = 20$ pA. The theoretical and experimental d axes are related through the known value of the statistic monomer size $a = 0.35$ nm by $d = d^* \times a$. The inset shows the tip-to-substrate cycling motion of the Fc heads of the chains, giving rise to the elastic bounded positive feedback current.

reaches a stationary velocity V_l and:

$$\frac{k_BT}{C_p}\frac{\partial C_p}{\partial x} + k_{spr}(x - x_e) + k_{dr}V_l = 0$$

The flux $J_{x,t}$ of Fc at time t through the plane located at the distance x from the electrode surface is given by $J_{x,t} = C_pV_l$, and the above equation leads to the following expression for the flux under conditions of elastic bounded diffusion:

$$J_{x,t} = -\frac{k_BT}{k_{dr}}\frac{\partial C_p}{\partial x} - \frac{k_{spr}}{k_{dr}}C_p(x - x_e) = -D\left(\frac{\partial C_p}{\partial x} + \frac{k_{spr}}{RT}C_p(x - x_e)\right) \quad (1)$$

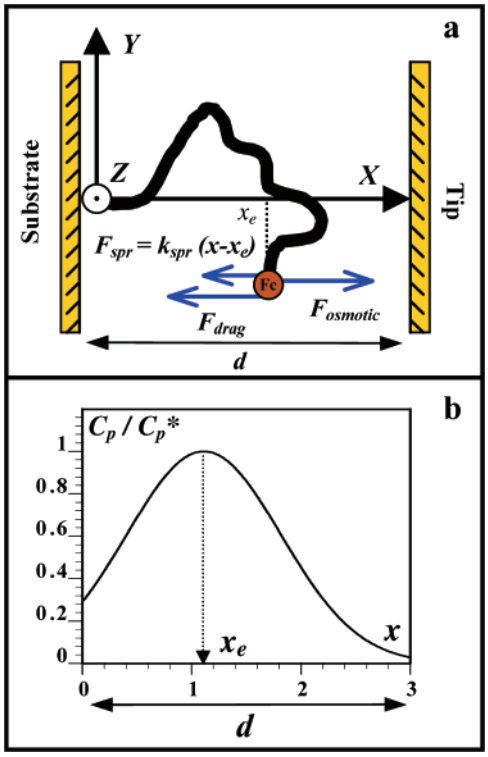

Figure 4. Depiction of the elastic bounded diffusion model. The Fc-PEG chain is end grafted onto the substrate surface and confined in the tip−substrate planar gap of width d. (a) The forces acting on the chain Fc head are: F_{spr}, a spring-like restoring force arising from the elasticity of the chain, F_{drag}, the frictional force that the Fc head has to overcome during its motion, $F_{osmotic}$, which results from the Fc head concentration gradient. The model introduces two parameters: x_e, the resting position of the Fc head within the Fc-PEG layer and k_{spr}, the spring constant of the chain. (b) The concentration profile of the ferrocene heads in the tip−substrate gap predicted by the model is Gaussian shaped and reaches its maximum for $x = x_e$.

the diffusion coefficient D of the chain head being related to the drag coefficient by the Einstein relation ($D = k_BT/k_{dr}$) and the spring constant k_{spr} being then defined as a molar quantity.

The following Fick-type equation then expresses the dynamics of the ferrocene heads in terms of their time- and space-dependent volume concentration within the tip−substrate gap:

$$\frac{\partial C_p}{\partial t} = -\frac{\partial J_{x,t}}{\partial x} = D\left\{\frac{\partial^2 C_p}{\partial x^2} + \frac{k_{spr}}{RT}\frac{\partial (C_p(x - x_e))}{\partial x}\right\} \qquad (2)$$

A similar equation has been used to describe the end-to-end dynamics of polymer chains in solution.[25] Such an harmonic spring model of a polymer chain was shown to capture the essential physics of chain dynamics.[26] More general models of this type, describing chain motion as diffusion under a conformational force field, are typically used to access the dynamics of chain segments of flexible biomolecules from fluorescent energy transfer measurements.[3c]

Because chain motion is fast with respect to the tip approach speed (microsecond vs second time scales), the recorded current is time independent (i.e., $\partial C_p/\partial t = -\partial J/\partial x = 0$) so that stationary values of J and $C_p(x)$ can be obtained by integration of the differential eq 2 as follows.

When no current flows (i.e., no anodic potential is applied to the tip) $J = 0$ and resolution of the first-order linear differential eq 1 yields:

$$C_p^0(x) = C_p^* \exp\left[-\frac{k_{spr}}{2RT}(x - x_e)^2\right]$$

with $C_p^* = C_p^0\ (x = x_e)$ as the integration constant.

C_p^*, the concentration profile of Fc heads at $x = x_e$, can be found by integration of $C_p^0(x)$ for every x value ranging from $x = 0$ up to $x = d$, which yields the surface concentration of Fc heads Γ: $\int_{x=0}^{d} C_P^0(x)\, dx = \Gamma$. From this, it ensues that

$$C_p^* = \Gamma / \int_{x=0}^{x=d} \exp\left[\frac{k_{spr}}{2RT}(x - x_e)^2\right] dx$$

The ferrocene head concentration profile at equilibrium within the layer is thus predicted to be given by a Gaussian curve centered on the value of $x = x_e$ (see Figure 4b), the width of this Fc head distribution profile being controlled by the chain spring constant.

When the potentials applied to the tip and the substrate are respectively positive and negative enough compared to the standard potential of the Fc/Fc^+ redox couple, a current will flow thru the system (J = constant).

At the tip ($x = d$), the Fc heads (noted P) are oxidized to ferrocenium Fc^+ ions (noted Q), that is:

$$P \rightarrow Q + e^- \text{ and thus } C_p(x = d) = 0$$

Whatever x, Q and P heads concentrations are related by a conservation equation:

$$C_p(x) + C_Q(x) = C_p^0(x)$$

At the substrate ($x = 0$), Q heads are reduced back to their P forms:

$$Q + e^- \rightarrow P \text{ and thus } C_Q(x = 0) = 0$$

$$\text{hence } C_p(x = 0) = C_p^0(x = 0)$$

By using these boundary conditions, integration of the differential eq 2 then yields the following expression for the elastic bounded SECM positive feedback current approach curve:

$$i = FSJ = FSD\Gamma\left[\int_0^d \exp\left(-\frac{k_{spr}}{2RT}(x - x_e)^2\right)\partial y \times \int_0^d \exp\left(\frac{k_{spr}}{2RT}(x - x_e)^2\right)\partial y\right]^{-1} \qquad (3)$$

with S the planar tip surface.

In the simple planar thin cell configuration depicted here, integration of the elastic bounded diffusion equations thus allows an analytical expression to be obtained, giving the Faradaic current i as a function of d, the tip−substrate separation. However calculation of the approach curve requires that the values of x_e and k_{spr} are known.[27] The most suitable configuration for deriving these quantities is the mushroom configuration, the one specifically addressed in the present work, for which the chains are grafted sufficiently far apart to neglect lateral interaction between them, so that only the behavior of a *single* isolated chain has to be modeled. In the present case, the elasticity of the PEG chain is of entropic nature, i.e., it solely depends on the number of conformations available to the chain for the random orientation of its monomers. As a result, chain attachment and confinement are expected to affect the chain overall conformation and flexibility. Unfortunately, no exact theoretical expression predicting the values of the parameters

x_e and k_{spr} for chains of finite length, attached to an interface and confined within a slab, is available. However, the equilibrium concentration profile of the end-grafted, confined, isolated polymer chains can conveniently be accessed by running Monte Carlo simulations, from which x_e and k_{spr} can be derived as follows.

Self-Avoiding Walk (SAW) Monte Carlo Simulations of the Equilibrium Conformation of End-Grafted Isolated Fc-PEG Chains. As the contour length of the PEG chain considered here, given by $L = Na = 28$ nm, greatly exceeds the statistical monomer size, $a = 0.35$ nm, the PEG chain can be modeled as a freely jointed chain.[23] The chain conformation can therefore be appropriately simulated by a three-dimensional random walk, reproducing the random orientation of the chain segments. The so-called excluded volume interactions (i.e., the repulsion between monomers), characterizing "real" chains in good solvents,[23] are taken into account by making the random walk self-avoiding[18] (see Experimental Methods).

Three-dimensional Monte Carlo simulations were run by generating randomly a large number of chain conformations, disposing the $N = 80$ successive monomers of the chain on a cubic lattice, following a self-avoiding walk starting at the chain anchoring point ($x = 0$, $y = 0$, $z = 0$) (see Figure 5a). The anchoring surface is the $Y-Z$ plane, and the tip is represented by an infinite plane perpendicular to the X axis and located at $x = d$. The grid spacing corresponds to a, the statistical monomer length of PEG. The monomers are confined in the tip−substrate gap and assumed to have no adsorption affinity for either surfaces. All the distances x, d, x_e, ... are normalized by a to yield their dimensionless counterparts: x^*, d^*, x_e^*, ...

We first address the conformation of the attached but unconfined chain. Averaging over all the conformations allows accessing the statistical size of the chain, i.e., its root-mean-square end-to-end distance R_F^*; as expected, we find $R_F^* \sim 15.6$, which is close to the size of the chain in solution, given by: $R_F^* = R_F/a \sim N^{0.6} = 13.8$. Even though the overall size of the chain is not much affected by attachment, end-grafting of a polymer chain is predicted to result in an elongation of the chain in the direction perpendicular to the grafting surface.[28] For the continuous chain limit (i.e., $N \rightarrow +\infty$, $a \rightarrow 0$), scaling laws predict that the mean square coordinate of the free end of the chain in the direction perpendicular to the surface ($\langle X^2 \rangle$) is twice the one in the direction parallel to the surface ($\langle Y^2 \rangle$), i.e., $\langle X^2 \rangle / \langle Y^2 \rangle = 2$.[29] The MC simulations we ran showed that, for a chain of a finite length of $N = 80$ monomers, this effect is significantly smaller because we found a ratio of $\langle X^2 \rangle / \langle Y^2 \rangle = 1.55$. The $\langle X^2 \rangle / \langle Y^2 \rangle$ ratio was however found to tend asymptotically toward its limiting value of 2 for somewhat longer chains ($N > 100$) (see Supporting Information). Sampling over a large number of conformations (typically more than 10^5) allows the three-dimensional (3D) ferrocene head equilibrium distribution to be derived. A cross-section of the 3D Fc head distribution along the X^*-Y^* plane, i.e., perpendicular to the anchoring surface, is shown in Figure 5b in the case of an unconfined chain (i.e. $d^* \gg R_F^*$). It is seen that the Fc head explores a roughly hemispherical volume centered around the X-axis, accordingly the average values of the y^* and z^* coordinates are: $\langle Y^* \rangle = \langle Z^* \rangle = 0$. The highest probability of finding the Fc head being thus located directly above the anchoring point, some $x = (8-9)a \sim 3$ nm away from the surface. As the AFM-SECM experiments address the motion of the Fc head perpendicular to the substrate, we are solely interested in the Fc head distribution along the dimension X. The equilibrium distribution of the x-coordinate of the Fc head position is shown in Figure 6 for an unconfined chain (part a) and for a chain under increasing confinement (parts b to d). We see that the equilibrium distribution of the x-coordinate of the Fc head position is always reasonably Gaussian shaped, not only for the unconfined chain (i.e., $d^* \gg R_F^*$) but also for all tip−substrate separations. This result demonstrates that the grafted chain considered here can indeed be assimilated to an harmonic spring, thus validating the basic postulate of the elastic diffusion model. Therefore, fitting the simulated profile by a Gaussian expression of the type: $p(x^*) \sim \exp[-k_{spr}a^2/2RT(x^* - x_e^*)^2]$, with $p(x^*)$ the probability density of the Fc head at the coordinate x, allows the value of both the effective chain spring constant and equilibrium head position to be determined for any value of d^*. The effect of confinement on the effective chain spring constant $k_{spr}^* = k_{spr}a^2/RT$ and on the chain-head equilibrium position x_e^* is shown in Figure 7. From the region of the curve corresponding to $d^* \gg R_F^*$, a value of $(1.48 \pm 0.02) \times 10^{-2}$ is obtained for the effective spring constant of the unconfined end-grafted chain. This value is comparable to the one expected for a real chain of the same length in solution, given by:[30] $k_{spr}^{*,sol} = k_{spr}^{sol}a^2/RT = 3/N^{6/5} \sim 1.56 \times 10^{-2}$, showing that terminal attachment does

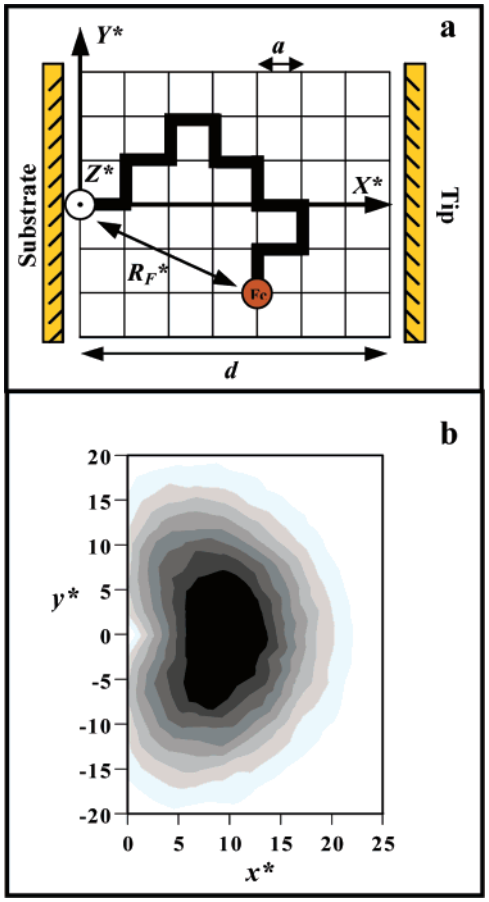

Figure 5. 3D Monte Carlo simulations of the equilibrium conformation of an end-grafted and confined Fc-PEG chain. (a) The simulated chain consist of N monomers disposed in a cubic lattice starting from the anchoring point of the chain and following a self-avoiding-random walk (SAW). The lattice size is a, the statistical monomer length. The asterisk indicates that all lengths are scaled to a. Average chain dimensions, such as the end-to-end distance R_F^*, can be obtained from the simulations. The represented chain is only $N = 12$ monomers long, the one actually simulated consists of $N = 80$ monomers. (b) Cross-section along the X^*-Y^* plane of the three-dimensional Fc head distribution, simulated in the case of an unconfined chain (i.e., $d^* \gg R_F^*$). Dark zones and light zones correspond respectively to a high and a low probability density of Fc head.

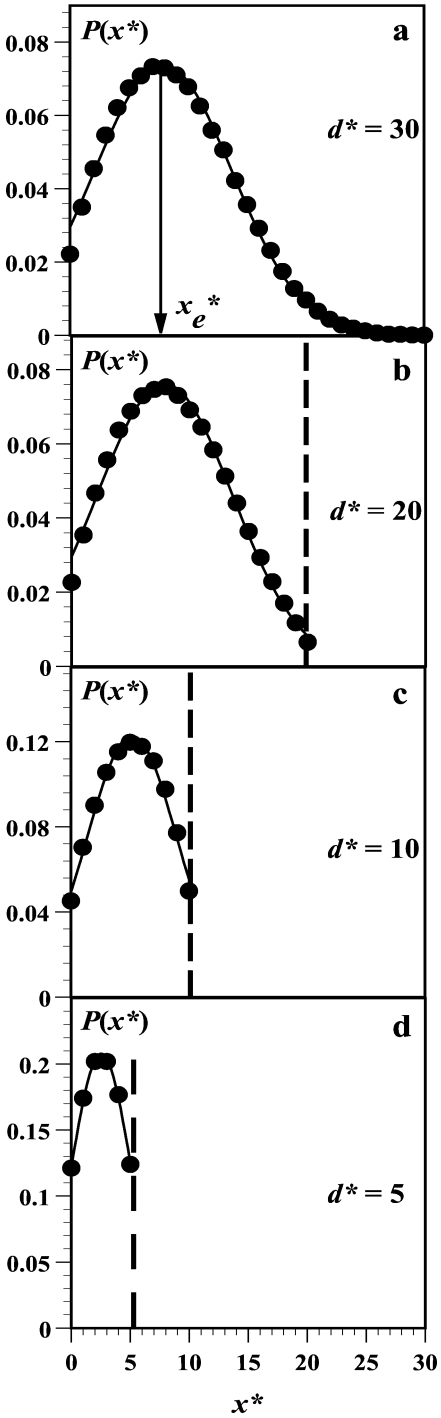

Figure 6. Equilibrium distribution of the Fc head along the x^* coordinate (perpendicular to the anchoring surface). The symbols correspond to the probability, density $p(x^*)$ of Fc head at coordinate x^* as derived from 3D Monte Carlo simulations run for the tip−substrate separation values d^* indicated near each curve. The dashed vertical line represents the surface of the confining tip. The chain confinement increases from (a), where the chain is unconfined, to (d). The continuous curves correspond to the best fit of the distribution profiles by a Gaussian expression, $p(x^*) \sim \exp[-k^*_{spr}(x^* - x^*_e)^2]$, from which the values of x^*_e, the chain head resting position, and k^*_{spr}, the chain effective spring constant, are derived.

not modify the effective elasticity of the chain considered here, whose actual spring constant remains close to ~0.5 pN/nm. However, it is also seen from Figure 7 that, when the chain is confined within a tip−substrate gap smaller than R^*_F, its effective elasticity decreases (i.e., k^*_{spr} increases) as a result of

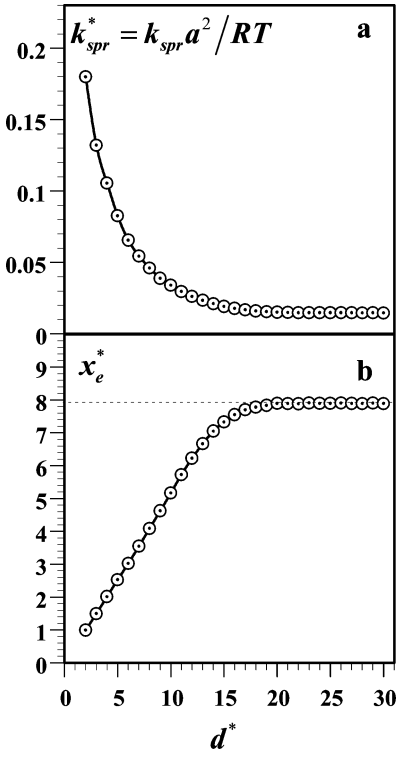

Figure 7. Dependence of (a) the effective spring constant of the chain, k^*_{spr} and (b) of the Fc head resting position, x^*_e, as a function of the confining tip-to-substrate distance d^*. The k^*_{spr} and x^*_e values are derived from the Monte Carlo simulations of the chain equilibrium conformation using the Gaussian fitting process schematized in Figure 6 and discussed in the text.

the decreasing number of possible chain conformations. Concomitantly the equilibrium position of the Fc head shifts from its position for the unconfined chain ($x^*_e = 7.9$) to the middle of the tip−substrate gap, i.e., $x^*_e = d^*/2$, as illustrated by the linear variation of x^*_e vs d^* seen in Figure 7b.

Once the values of k^*_{spr} and x^*_e are known for any value of d^*, the analytical expressions derived above by using the elastic bounded diffusion model can then be used to calculate the dimensionless SECM positive feedback approach curves from eq 3 yielding:

$$\Psi = \frac{i}{i_0} = \left[\int_0^{d^*} \exp\left(-\frac{1}{2}k^*_{spr}(x^* - x^*_e)^2\right) \partial x^* \times \int_0^{d^*} \exp\left(\frac{1}{2}k^*_{spr}(x^* - x^*_e)^2\right) \partial x^*\right]^{-1} \quad (4)$$

with $i_0 = FSD\Gamma/a^2$ a current characterizing the chain dynamics. As seen in Figure 8, the above equation predicts that a current should be detected for tip−substrate separations $d^* < 15$, i.e., below the size of the grafted chain. The elastic bounded positive feedback current is then expected to rise continuously upon further approach of the tip from the substrate. At very close tip−substrate separation (i.e., $d^* \rightarrow 0$), and $x^*_e \rightarrow d^*/2$ (see Figure 7b), eq 4 then tends toward: $\Psi = 1/d^{*2}$, meaning that the actual current is then given by $i = FSD\Gamma/d^2$. This expression is the one expected for a species undergoing simple free diffusion in a narrow slab. Therefore, despite the elastic nature of the chain, at very close tip−substrate separation, a diffusion-like regime is reached.

The above general expression for the bounded positive feedback current is valid for the case of a planar tip approaching a planar substrate bearing flexible chains. Yet in the present

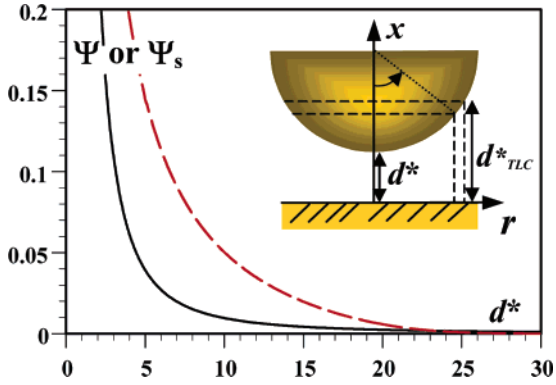

Figure 8. Theoretical positive feedback approach curves calculated using the formalism of the elastic bounded diffusion model and the results of Monte Carlo simulations for an end-grafted chain of $N = 80$ monomers. The dimensionless tip current, denoted Ψ for a planar tip (eq 4) and Ψ_s (eq 5) for a spherical tip, is plotted as function of the dimensionless tip−substrate separation $d^* = d/a$. The dimensionless tip current is defined as the i/i_0 ratio, with i the actual current and i_0 a current characterizing the chain dynamics, given by $i_0 = FSD\Gamma/a^2$ for a planar tip and $i_0 = 2\pi FDR_{tip}\Gamma/a$ for a large spherical tip of radius R_{tip}. a is the monomer statistical length, Γ is the chain surface coverage, and D the effective diffusion coefficient of the chain head. The inset shows how the surface below the spherical tip is divided into an elementary concentric ring of radius r, each of them acting as a planar thin layer cell of height d_{TLC}, to derive the elastic bounded positive feedback response by integration of the feedback current (see text).

case, the tip used is an extremely smooth submicrometer-sized spherical electrode (see Experimental Methods). To accommodate for such a tip geometry, we need to integrate the above expression over the lower half surface of a spherical tip. This is carried out by dividing the tip and substrate in elementary concentric rings, as shown in the inset of Figure 8 and assuming that each ring forms an elementary planar thin layer cell, i.e., that the "diffusional" field is oriented perpendicularly to the substrate. This is justified by the very close tip−substrate separation required for the chains to reach the tip surface. Each thin layer cell is characterized by its thickness d_{TLC}, as defined in the inset of Figure 8, and by its surface ∂S given by: $\partial S = 2\pi R_{tip}[1 - (d_{TLC} - d)/R_{tip}]\partial d_{TLC}$, with R_{tip} the tip radius. Each cell therefore contributes to the current by an amount ∂i given by eq 3:[31]

$$\partial i = FD\Gamma\left[\int_0^{d_{TLC}} \exp\left(-\frac{k_{spr}}{2RT}(x - x_e)^2\right)\partial y \times \int_0^{d_{TLC}} \exp\left(\frac{k_{spr}}{2RT}(x - x_e)^2\right)\partial y\right]^{-1}\partial S$$

Integration of the contribution to the current of all of the cells that the chains can gap, i.e., for $d_{TLC} \leq L$, with L the fully elongated chain length, and taking into account that the tip is much larger than the chains (i.e., $(d_{TLC} - d)/R_{tip} \ll 1$), we obtain:

$$i = \frac{2\pi R_{tip}\Gamma FD}{a^2}\int_{d^*}^{L^*} \psi(d^*_{TLC}, k^*_{spr}, x^*_e)\,\partial d^*_{TLC},$$

Ψ being given by eq 4

Taking further into account that $L^* = L/a = N \gg 1$, we derive the following expression for the elastic bounded positive feedback dimensionless current Ψ_s at a large spherical tip:

$$\psi_s = \frac{i}{i^*} = \int_{d^*}^{+\infty} \psi\,\partial d^*_{TLC} \qquad (5)$$

with $i_0 = 2\pi FDR_{tip}\Gamma/a$ a characteristic current reflecting the chain dynamics.

Numerical evaluation of the above integral allows the elastic bounded positive feedback approach curve to be obtained for the spherical-tip-toward-planar-substrate situation by plotting ψ_s as a function of d^* (see dashed curve in Figure 8). As expected, the approach curve thus predicted is not quite as steep as the one derived in the case of a planar tip. Nevertheless, a marked current increase is also expected when $d^* < 20$. Interestingly, and as observed above for the case of a planar tip, at very low tip−substrate separations (i.e., $d^* \to 0$), a purely diffusive regime is reached and the current is then given by: $\psi_s = 1/d^*$, i.e., $i = 2\pi FDR_{tip}\Gamma/d$.

Determination of the Diffusion Coefficient of the Grafted Chains from the Elastic Bounded Diffusion Positive Feedback Response: Structural Characterization of the PEG Layer from the Force Curve. The theoretical elastic bounded diffusion approach curve can now be adjusted onto the experimental current approach curves using a *single* adjustable parameter, namely the characteristic current i_0, as the abscissa of the theoretical approach curves is immediately converted into a d scale using: $d = d^* \times a$ with $a = 0.35$ nm. We see in Figure 3b that the presented current approach curve can then be very satisfyingly fitted using the calculated elastic bounded SECM positive feedback curve, down to $d = 2$ nm, for $i_0 = 20$ pA. From the expression of i_0, i.e., $i_0 = 2\pi FDR_{tip}\Gamma/a$, knowing the tip radius and the surface coverage Γ, a value of $D = 10^{-8}$ cm^2/s can be derived for the diffusion coefficient of the Fc head of the PEG chain. Considering all of the recorded approach curves, an average value of $(2 \pm 1) \times 10^{-8}$ cm^2/s is found for D. This diffusion coefficient reflects the overall frictional resistance experienced by the Fc head during its tip-to-substrate motion. The value found for D points to an additive friction of all of the monomers of the chain on the solvent because, in this case, a diffusion coefficient $D_{add} = D_m/N \sim 8 \times 10^{-8}$ cm^2/s is expected, with $D_m \sim 6 \times 10^{-6}$ cm^2/s the diffusion coefficient of the monomer.[8] We note, however, that the value we obtain for D is slightly lower than D_{add}. The above results indicate that the elastic bounded diffusion model, like any other models treating polymer dynamics as diffusion on a free-energy surface,[25,26] correctly describes the end-to-end dynamics of linear chains but yields an effective diffusion coefficient smaller than expected.[2a,32] The fundamental physical reason behind such a systematic underestimation is still actively debated.[32b]

Another interesting parameter that can be estimated from the current data is the number of chains involved in the generation of the Faradaic current. Considering that for $d = 2$ nm the exchange of a single electron would result in a current of $\sim eD/d^2 \sim 0.04$ pA (e being the charge of an electron), and as we recorded for this distance a current of $\sim$4.5 pA, it can be estimated that $\sim$100 chains generate the positive feedback current. This number is to be compared with the number of chains able to efficiently contact the tip for $d = 2$ nm, simply derived by geometric considerations: $n_c \sim \pi\Gamma\mathcal{N}R_{tip}(R_F - d) \sim 130$ chains, taking $R_{tip} = 225$ nm and $R_F \sim 5$ nm. This latter number of chains is indeed very similar to the one calculated above using the experimentally derived value of D, which is an indication of the validity of the elastic bounded diffusion model.

However, below 2 nm, it was consistently observed that the theoretical current approach curve derived above ceases to fit the data. The experimental current is then lower than expected, and a peak is observed that is not accounted for by the model. This issue is discussed below in further details.

Turning now to the force curve, we see, as represented in Figure 3a, that a very good quantitative fit of the exponential decay of the force with distance can be obtained, using the theoretical force law predicted for the compression of polymer mushroom by a spherical tip, given by:[33] $F \approx 72\pi R_{tip}\Gamma RT \exp[-d/R_{chain}]$ and taking for R_{tip} and Γ their experimental values. The only adjustable parameter is then the characteristic force decay length R_{chain}, for which we find a best fit value of $\sim$ 4 nm. Even though the above force vs distance expression was initially derived for the compression of ideal chains, its use was shown to yield reasonable estimates for the size of real chains in good solvent conditions.[34] Likewise, the R_{chain} value we find here is close to the Flory radius of the grafted chains we derived from our MC simulations ($R_F \sim 5$ nm). This agreement confirms that the chains are homogeneously grafted on the surface in a mushroom configuration. However, as was observed for the current approach curve, the above theoretical expression ceases to fit the force data for d below 2 nm, the force required to further compress the layer increasing rapidly. The very fact that such a transition was observed both on the force and current approach curves seems to indicate that, below this critical compression distance, the chain undergoes some abrupt conformation change that makes it stiffer and concomitantly reduces its dynamics.

Origin of the Peak in the Current Approach Curves. Among the possible causes for the recorded decrease of tip current with decreasing tip-to-substrate distance is the compression-induced detachment of the chains from the surface. However, as shown in Figure 2b, the positive feedback curve recorded when the tip is retracted away from the surface is similar both in shape and intensity to the one recorded upon approach of the tip, indicating that no material is lost upon compression. The observed decrease of the positive feedback current at close tip−substrate separation thus rather points to a slowing of chain dynamics upon compression. Confinement of the chains in the tip−surface gap results in a local increase in the chain concentration accompanied by a rising of both the local viscosity[23a] and the degree of self-entanglement of the chains.[35] Understandably, both effects combine to lead to a gradual loss of the chain mobility upon increasing compression. Within the framework of the elastic bounded model, chain dynamics is characterized by a diffusion coefficient, therefore, a slowing in chain dynamics is to be represented by a decreasing diffusion coefficient. To the best of our knowledge, no workable expression exists to quantify this compression-induced slowing of diffusion. In an attempt to assess semiquantitatively the effect of this confinement-induced chain mobility loss and to see if it can result in a peak-shaped approach curve, we thus introduce a tip−substrate distance-dependent diffusion coefficient given by a step function, which is the steepest possible variation of D with d:

$$\begin{cases} d \geq d_c: & D = cte \\ d < d_c: & D = 0 \end{cases}$$

with d_c a critical compression distance below which chain motion is totally hindered.

According to this model, below a characteristic confinement distance d_c, the diffusion coefficient of the chains abruptly drops to zero (see upper part of Figure 9).

Numerical evaluation of the integral eq 5, taking into account this distance-dependent diffusion coefficient, allows the approach curve presented in Figure 9 (dashed curve) to be calculated. As can be seen, introduction of a steplike variation of the diffusion coefficient only results in a leveling of the current approach curves for $d < d_c$ and not in a peak-shaped approach curve. This behavior finds its origin in the use of large tips for which the expression of the positive feedback current becomes independent from the tip−substrate separation d^*, and only depends on d_c^*, as from eq 5:

$$\psi_s = \int_{d^*}^{+\infty} \psi\, \partial d^*_{TLC} = \int_{d^*}^{d_c^*} \psi\, \partial d^*_{TLC} + \int_{d_c^*}^{+\infty} \psi\, \partial d^*_{TLC} = \int_{d_c^*}^{+\infty} \psi\, \partial d^*_{TLC}$$

because for $d < d_c$, $D = 0$ and $\psi = 0$.

The physical reason behind this predicted leveling-off of the current is as follows. As the tip is approached from the surface by a small amount Δd, the chains, located at a radial distance r_c from the tip axis, and initially "seeing" the tip under a distance d_c, are "frozen" by overcompression, while the neighboring chains, located at $r_c + \Delta r$, are brought to a distance d_c from the tip (see Inset of Figure 8). Because the electrode is very large, there are as many chains of both types, therefore, their contribution to the overall current perfectly compensates and the current remains constant as d is decreased.[36]

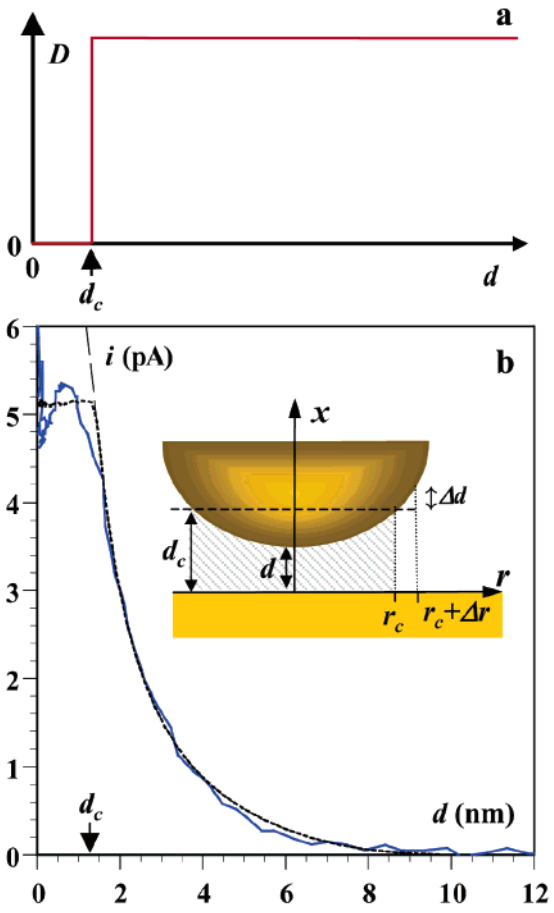

Figure 9. Effect of introducing a confinement-induced slowing of the chain dynamics on the theoretical current approach curve. (a) A step function is assumed for the diffusion coefficient of the chain, which reflects the chain dynamics within the elastic bounded diffusion model: the motion of the chains compressed within a tip−substrate gap thinner than some critical width value d_c, is assumed to be totally hindered, i.e, $D = 0$ for $d < d_c$. (b) The resulting theoretical current approach curve, calculated taking $d_c = 4a = 1.4$ nm (dotted curve), is compared to the curve derived from eq 5, which ignores compression-induced chain slowing (dashed curve), and to the experimental approach curve (continuous line). Conditions are as in Figure 2. The inset depicts the tip−substrate gap, the dashed area corresponds to the zone where the tip−substrate separation is below d_c, i.e, in this zone, $D = 0$.

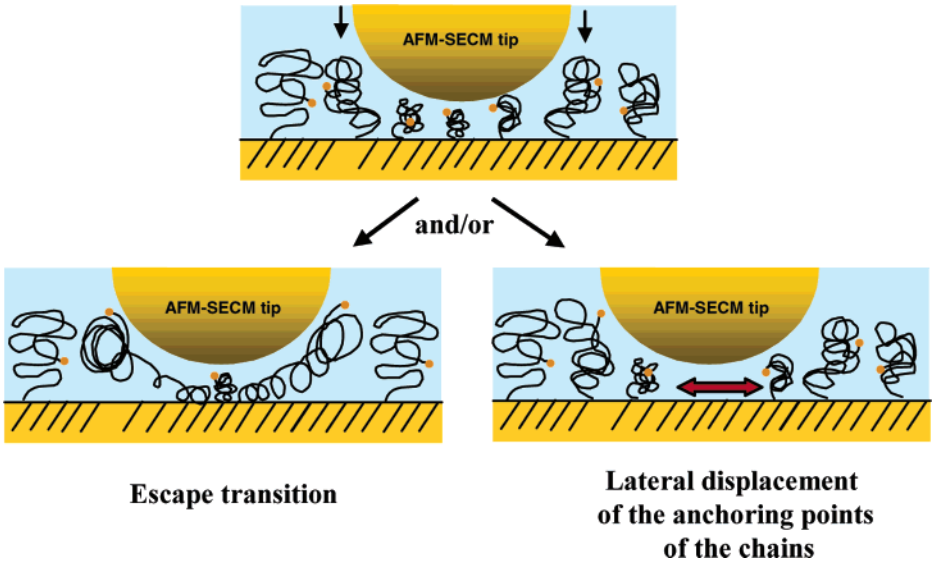

Figure 10. Possible mechanisms for the compression-induced escape of the chains from within the narrowing tip−substrate gap. (Left) The chain simply elongates while remaining anchored at the same location of the surface. (Right) The anchoring bond of the chain moves along the surface.

The above results show, on the basis of the steepest possible variation of the chain dynamics (i.e., diffusion coefficient) with distance, that confinement-induced slowing of individual chains cannot justify *by itself* the presence of a peak in the current approach curve. However, the situation is expected to differ greatly if it is assumed that the overcompressed chains not only "freeze" but also come to interact (entangle) with neighboring chains, thus slowing *their* dynamics. In such a case, the slowing phenomenon propagates *laterally*, and at the opposite of the situation depicted above, the contribution of the "frozen" chains to the overall current cannot be compensated by the one due to the neighboring chains because the latter now display *slower* dynamics than unperturbed chains. The current is then understandably expected to decrease with decreasing tip−substrate separation. Interaction between neighboring chains implies that, upon compression, the grafted chains are able to stretch out to reach their neighbors while laterally escaping from the narrowing tip−substrate gap. One can envision two mechanisms for such an escape phenomenon (Figure 10): either the chain simply elongates while remaining anchored at the same location of the surface (Figure 10, left), or the anchoring bond of the chain is displaced along the surface (Figure 10, right). The latter escape mechanism is supported by the fact that the motion of thiol-adsorbed molecules along gold surfaces has already been reported, even though this process was shown to be very slow.[37] The former mechanism corresponds to the so-called escape transition of a linear chain compressed by a solid obstacle and has been predicted theoretically,[38,39] even though it has never been observed experimentally. Escape transition is expected to occur either when the dimension of the confining surface is smaller than the length of the fully elongated chain,[38] or when the chain is compressed between a curved surface an a plane,[39] such as is the case here.

Monte Carlo simulations were run in order to assess the effect of such an escape transition on the ferrocene head concentration profile within the spherical-tip substrate gap.

Monte Carlo Simulations of the PEG Chain Escape Transition: Effect on the Fc Head Concentration Profile. 3D Monte Carlo simulations were run as described above except that the planar tip was replaced by a large spherical tip having a diameter of $R_{tip} = 225$ nm $= 640\ a$, such as the one experimentally used. The anchoring points of the chains on the surface were disposed in a square lattice with a spacing of 5.8 nm $\sim 17\ a$, corresponding to the actual surface coverage of $\Gamma = 5 \times 10^{-12}$ mol cm^{-2}. The tip was assumed to approach the surface along the X^* axis directly above a grafted chain. The conformation of an isolated chain, grafted on the surface along the Y^* axis, at increasing radial distances from the tip axis, was simulated for several tip−substrate separations d^* (see Figure 11, representing the case $d^* = 0$). The effect of the escape transition phenomenon on the distribution of the y^* coordinate of the Fc heads of anchored chains is exemplified in the inset of Figure 11 for a chain grafted on the surface in site 6. It is seen that instead of being symmetrical with respect to the position of the anchoring point of the chain (indicated by a thick green line), as would be the case for an uncompressed chain, or a chain compressed by a large planar tip, the distribution profile is significantly shifted aside from the anchoring point. The chain head is found at y_0^* coordinates significantly exceeding the coordinate of the anchoring point, $y_0^* = 85$. This means that a large fraction of the chain conformations are escaped, i.e., that the Fc head is not located above the chain-anchoring point but further away from the tip axis within a region of space where the tip−substrate gap is larger. Moreover, the chain then largely reaches out to the anchoring position of the neighboring chain ($y_0^* = 102$, marked by a red dotted line in the inset of Figure 11). The dependence of the escape phenomenon on chain compression can be further quantified by deriving from the MC simulations the value of ΔY^*, the mean y^* coordinate of the Fc head with respect to the chain anchoring point: $\Delta Y^* = \langle Y^* \rangle - y_0^*$, for various tip−substrate separations (see Figure 11). A value of $\Delta Y^* = 0$ is expected for a nonescaped chain, while the more the chain escapes, the larger the ΔY^* value. Figure 12 shows the variation of ΔY^* with d^* calculated for individual chains grafted on the surface at sites 1, 3, 5, 6, 7, 8, and 10 (as defined in Figure 11). It is seen that the chains located either directly below the tip (site 1) or far from the tip axis (site 10) are not escaped whatever d^*. In the latter case, the chain is sufficiently far away from the tip axis to behave as an unescaped chain, while in the former case, the chain is totally confined below the very end of the tip from which it cannot escape even when fully elongated. At the opposite, for the chains in sites 3−7, it is seen that escape transition becomes significant for $d^* < 6$, i.e., for a tip−substrate separation of ~2 nm. Considering the fact that site 7 corresponds

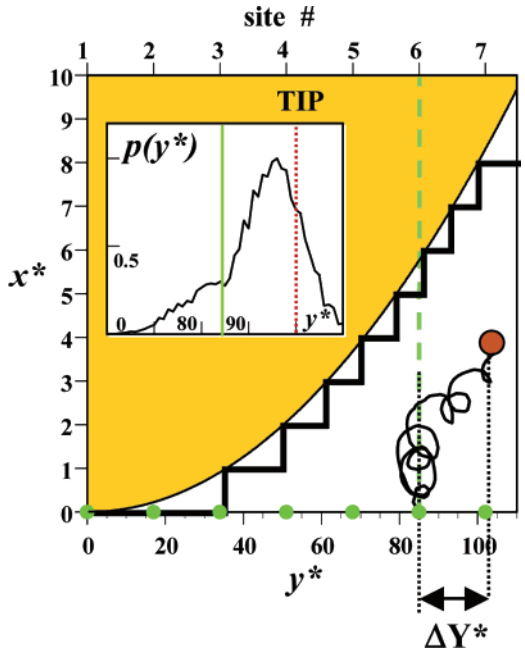

Figure 11. Monte Carlo simulations of the PEG chain escape transition. The tip approaches the surface along the X^* axis directly above a grafted chain; in the case presented here, the tip is in contact with the substrate, i.e., $d^* = 0$. The conformation of isolated chains grafted on the surface along the Y^* axis, at increasing radial distances from the tip axis, is simulated. The anchoring points of the chains are represented by green dots on the lower axis of the graph. Each grafting site is labeled 1−7 as shown by the upper axis of the graph. The chain in site 6, grafted at the y^* coordinate $y_0^* = 85$, is represented schematically together with the position of its Fc head (not on scale). The inset shows the distribution of the y^* coordinate of the Fc head of the chain grafted in site 6. The green line represents the coordinate of the anchoring point of the chain, while the red dotted line shows the grafting position of the neighboring chain, grafted in site 7 ($y_0^* = 102$).

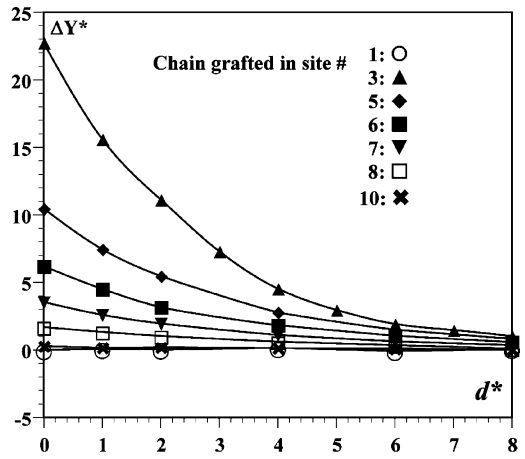

Figure 12. Magnitude of the escape phenomenon of compressed chains as a function of the confining distance d^* for chains grafted on the surface at sites located at increasing radial distances from the tip axis (sites 1−10 as defined in Figure 11). The magnitude of the escape phenomenon is quantified by ΔY^*, defined as the mean y^* coordinate of the chain Fc head with respect to the chain-anchoring point, i.e., $\Delta Y^* = \langle Y^* \rangle - y_0^*$. A value of $\Delta Y^* = 0$ is expected for a nonescaped chain, while the more the chain escapes, the larger the ΔY^* value.

to a radial distance from the tip center of $6 \times (17a) \sim 36$ nm, it can be estimated that only the chains located directly below the tip and within a radius of the tip axis of $r \sim 36$ nm undergo a significant escape transition. The corresponding number of escaped chains, n_e, can be estimated from $n_e = \pi r^2 \Gamma \mathcal{N} \sim 130$, which interestingly amounts for all of the chains calculated above to participate in the positive feedback process.

The above results demonstrate that, in the very conditions of the here-reported experiments (tip size, chain coverage), confinement-induced chain escape is indeed expected to happen and that grafted chains do elongate laterally to such an extent that they can interact with their neighbors, a prerequisite for the occurrence of a peak in the current approach curve (see above). Moreover, the chain escape is predicted to occur at tip−substrate separations below ∼2 nm, a region for which a peak is indeed observed in the experimental approach curve. Finally, it is demonstrated that *all* of the chains generating the positive feedback current are expected to undergo a significant escape transition within this tip−substrate range. All of the above is a strong indication that the peak in the current approach curve finds its origin in the escape transition of the chains. Nevertheless, it is not possible on the sole basis of the reported data, to exclude the occurrence of surface displacement of the anchoring point of the chains along the gold surface as an alternative or parallel mechanism for chain escape.

Conclusion

We have shown here that the dynamics of nanometer-sized, linear polymer chains, end-tethered to a surface in a mushroom conformation, can be quantitatively probed by AFM-SECM at the scale of ∼100 molecules. Upon approach of the microelectrode tip from the anchoring substrate, to within a distance comparable to the chain dimension, recording of the force approach curve gives access to the chain overall conformation, while the tip current response yields access to the chain dynamics, providing a suitable model describing the motion of the Fc-labeled free end of the chain is used. The elastic bounded diffusion model, which we proposed earlier and further developed here, provides such a theoretical tool. It considers the motion of the ferrocene head of the chain as a diffusion process in a potential field governed by a Fick-type equation. The conformational potential field is derived from the equilibrium conformation of the chain, which is accessed by Monte Carlo (MC) simulations. It is shown that, for the relatively short end-grafted chain considered here ($N = 80$), the conformational field is approximately parabolic, i.e., that the chain can be modeled as an harmonic spring. The effective spring constant of the chain and the equilibrium position of the ferrocene head can be derived from MC simulations for any degree of chain confinement, and the complete theoretical SECM current approach curve can then be calculated. For tip−substrate separations larger than ∼2 nm, the experimental current approach recorded curve can be very satisfyingly reproduced by theory using only one adjustable parameter characterizing the chain dynamics, the effective diffusion coefficient D of the chain head. The thus derived a value of $D \sim 2 \times 10^{-8}$ cm^2/s points to an addictive friction of the chain monomers.

For tip−substrate separations shorter than ∼2 nm, the experimentally observed occurrence of a peak in the current approach curve, which is not predicted by the developed model, indicates that the initially well-separated chains come to interact with their neighbors when overcompressed, thus slowing their dynamics. This in turn implies that the chains are capable of avoiding overcompression by escaping the narrowing tip−substrate gap, either by chain elongation or lateral displacement of the chains' anchoring points along the surface. MC simulations provide quantitative indications that the chains generating the Faradaic current indeed undergo significant lateral chain elongation at high compression.

Supporting Information Available: Figures showing the variation with chain length of the end-to-end distance and of the aspect ratio of the end-attached chains, as derived from the simulations reported in this work. Expression of the elastic bounded positive feedback current at a spherical tip of finite radius. This material is available free of charge via the Internet at http://pubs.acs.org.

References and Notes

(1) Wagner, P. J.; Klán, P. *J. Am. Chem. Soc.* **1999**, *121*, 9626−9635.

(2) (a) Wallace, M. I.; Ying, L.; Balasubramanian, S.; Kelerman, D. *Proc. Natl. Acad. Sci. U.S.A.* **2001**, *98*, 5584−5589. (b) Bonnet, G.; Krichevsky, O.; Libchaber, A. *Proc. Natl. Acad. Sci. U.S.A.* **1998**, *95*, 8602−8606. (c) Du, Q.; Smith, C.; Shieldrim, N.; Vologodskaia, M.; Vologodskii, A. *Proc. Natl. Acad. Sci. U.S.A.* **2005**, *102*, 5397−5402. (d) Ansari, A.; Kuznetsov, S.; Shen, Y. *Proc. Natl. Acad. Sci. U.S.A.* **2001**, *98*, 7771−776. (e) Kawai, K.; Yoshida, H.; Sugimoto, A.; Fujitsuka, M.; Majima, T. *J. Am. Chem. Soc.* **2005**, *127*, 13232−13237. (f) Trifonov, A.; Raytchev, M.; Buchvarov, I.; Rist, M.; Barbaric, J.; Wagenknecht, H.-A.; Fiebig, T. *J. Phys. Chem. B* **2005**, *109*, 19490−19495.

(3) (a) Haas, E.; Wilchek, M.; Katchalski-Katzir, E.; Steinberg, I. Z. *Proc. Natl. Acad. Sci. U.S.A.* **1975**, *72*, 1807−1811. (b) Bieri, O.; Wirz, J.; Hellrung, B.; Schutkowski, M.; Drewello, M.; Kiefhaber, T. *Proc. Natl. Acad. Sci. U.S.A.* **1999**, *98*, 9597−9601. (c) Hass, E. *ChemPhysChem* **2005**, *6*, 858−870. (d) Schuler B. *ChemPhysChem* **2005**, *6*, 1206−1220. (e) Michalet, X.; Weiss, S.; Jäger, M. *Chem. Rev.* **2006**, *106*, 1785−1813.

(4) (a) Fytas, G.; Anastasiadis, S. H.; Seghruochni, R.; Vlassopoulos, D.; Li, J.; Factor, B. J.; Theobald, W.; Toprakcioglu, C. *Science* **1996**, *274*, 2041−2044. (b) Monkenbush, M.; Schneiders, D.; Richter, D.; Farago, B.; Fetters, L.; Huang, J. *Physica B* **1995**, *213*, 707−711. (c) Zeghal, M.; Deloche, B.; Auroy, P. *Macromolecules* **1999**, *32*, 4947−4955. (d) Michailidou, V. N.; Loppinet, B.; Prucker, O.; Ruhe, J.; Fytas, G. *Macromolecules* **2005**, *38*, 8960−8962.

(5) (a) Macpherson, J. V.; Unwin, P. R. *Anal. Chem.* **2000**, *72*, 276−285. (b) Macpherson, J. V.; Webb, M. A.; Unwin, P. R. *Anal. Chem.* **2001**, *73*, 550−557. (c) Kranz, C.; Friedbacher, G.; Mizaikoff, B.; Lugstein, A.; Smoliner, J.; Bertagnolli, E. *Anal. Chem.* **2001**, *73*, 2491−2500. (d) Kranz, C.; Kueng, A.; Mizaikoff, B.; Lugstein, A.; Bertagnolli, E. *Angew. Chem., Int. Ed.* **2003**, *42*, 3238−3240.

(6) Binnig G.; Quate, C. F.; Gerber, C. *Phys. Rev. Lett.* **1986**, *56*, 930−933.

(7) (a) *Scanning Electrochemical Microscopy*; Bard, A. J., Mirkin, M. V., Eds.; Marcel Dekker: New York, 2001. (b) Bard, A. J.; Fan, F.-R. F.; Mirkin, M. V. In *Electroanalytical Chemistry*; Bard A. J., Ed.; Marcel Dekker: New York, 1994; Vol. 18, p 243.

(8) Abbou, A.; Anne, A.; Demaille, C. *J. Am. Chem. Soc.* **2004**, *126*, 10095−10108.

(9) (a) Anne, A.; Demaille, C.; Moiroux, J. *J. Am. Chem. Soc.* **1999**, *121*, 10379−10388. (b) Demaille, C.; Moiroux, J. *J. Phys. Chem. B* **1999**, *103*, 9903−9909. (c) Anne, A.; Demaille, C.; Moiroux, J. *J. Am. Chem. Soc.* **2001**, *123*, 4817−4825.

(10) (a) Alexander, S. *J. Phys.* **1977**, *38*, 983−987. (b) de Gennes, P. G. *Macromolecules* **1980**, *13*, 1069−1075.

(11) Anne, A.; Moiroux, J. *Macromolecules* **1999,** 32, 5829−5835.

(12) (a) Hegner, M.; Wagner, P.; Semenza, G. *Surf. Sci.* **1993**, *291*, 39−46. (b) Wagner, P.; Hegner, M.; Güntherodt, H.-J.; Semenza, G. *Langmuir* **1995**, *11*, 3867−3875.

(13) Anne, A.; Demaille, C.; Moiroux, J. *Macromolecules* **2002**, *35*, 5578−5586.

(14) (a) Michri, A. A.; Pshenichnikov, A. G., Burshtein, R. *Elektrokhimiya* **1972**, *8*, 364−366. (b) Rand, D. A. J.; Woods, R. *J. Electroanal. Chem.* **1972**, *35*, 209−218. (c) Cadle, S. H.; Bruckenstein, S. *Anal. Chem.* **1974**, *46*, 16−20. (d) Trasatti, S.; Petrii, O. A. *Pure Appl. Chem.* **1991**, *63*, 711−734.

(15) Abbou, J.; Demaille, C.; Druet, M.; Moiroux, J. *Anal. Chem.* **2002**, *74*, 6355−6363.

(16) Sader, J. E.; Chon, J. W. M.; Mulvaney, P. *Rev. Sci. Instrum.* **1999**, *70*, 3967−3969.

(17) Sader, J. E.; Larson, I.; Mulvaney, P.; White, L. R. *Rev. Sci. Instrum.* **1995**, *66*, 3789−3798.

(18) Sokal, A. D. In *Monte Carlo and Molecular Dynamics Simulations in Polymer Science*; Binder, K., Ed.; Oxford University Press: New York, 1995; p 47117.

(19) Rosenbluth, M.; Rosenbluth, A. *J. Chem. Phys.* **1955**, *23*, 356−359.

(20) (a) McCrackin, F. L. *J. Chem. Phys.* **1967**, *47*, 1980−1986. (b) Clayfield, E. J.; Lumb, E. C. *J. Colloid Interface Sci. Phys.* **1966**, *22*, 285−293.

(21) Jaeckel A.; Dayantis, J. *J. Phys. A: Math. Gen.* **1994**, *27*, 2653−2667.

(22) Laviron, E. In *Electroanalytical Chemistry*; Bard, A. J., Ed.; Marcel Dekker: New York, 1982; Vol. 12, pp 53−157.

(23) (a) Grosberg, A. Y.; Khokhlov, A. R. *Statistical Physics of Macromolecules*; American Institute of Physics: New York, 1994. (b) de Gennes, P. G. *Scaling Concepts in Polymer Physics*; Cornell University Press: Ithaca, NY, 1991.

(24) (a) Kenworthy, A. K.; Hristova, K.; Needham, D.; McIntosh, T. J. *Biophys. J.* **1995**, *68*, 1921−1936. (b) Hansen, P. L.; Cohen, J. A.; Podgornik, R.; Parsegian, V. A. *Biophys. J.* **2003**, *84*, 350−355.

(25) Szabo, A.; Schulten, K.; Schulten, Z. *J. Chem. Phys.* **1980**, *72*, 4350−4357.

(26) Wilemski, G.; Fixman, M. *J. Chem. Phys.* **1974**, *60*, 878−890.

(27) In our previous report (ref 8), we made the coarse simplifying assumption that $x_e = 0$ and used k_{spr} as an adjustable parameter.

(28) (a) Dimarzo, E. A.; McCrackin, F. L. *J. Chem. Phys.* **1965**, *43*, 539−547. (b) Rex, S.; Zuckerman, M. J.; Lafleur, M.; Silvius, J. R. *Biophys. J.* **1998**, *75*, 2900−2914.

(29) Eisenriegler, E.; Kremer, K.; Binder, K. *J. Chem. Phys.* **1982**, *77*, 6296−6320.

(30) Pincus, P. *Macromolecules* **1976**, *9*, 386−388.

(31) A similar calculation method has been successfully used to assess the effect of tip shape on SECM positive feedback response of solution species, see: (a) Davis, J.; Fan, F.-R. F.; Bard, A. J. *J. Electroanal. Chem.* **1987**, *238*, 9−31. (b) Mirkin, M. V.; Fan, F.-R. F.; Bard, A. J. *J. Electroanal. Chem.* **1992**, *328*, 47−62.

(32) (a) Lapidus, L. J.; Steinbach, P. J. Eaton, W. A.; Szabo, A.; Hofrichter, J. *J. Phys. Chem. B* **2002**, *106*, 11628−11640. (b) Portman, J. J. *J. Chem. Phys.* **2003**, *118*, 2381−2391. (c) Lapidus, L. J.; Easton, W. A.; Hofrichter, J. *Proc. Natl. Acad. Sci. U.S.A.* **2005**, *102*, 5397−5402.

(33) Israelachvili, J. *Intermolecular and Surface Forces*, 2nd ed.; Academic Press: San Diego, 1992; pp 288−311.

(34) Kuhl, T. L.; Leckband, D. E.; Lasic, D. D.; Israelachvili *Biophys. J.* **1994**, *66*, 1479−1488.

(35) Edvinsson, T.; Elvingson, C.; Arteca, G. A. *Macromol. Theory Simul.* **2000**, *9*, 398−406.

(36) For tips much smaller than the one used here (i.e., such as $R_{tip} \sim L$), the situation is obviously different, as the number of chains contributing to the overall current decreases rapidly from right below the tip axis toward the tip edge. Therefore, tip-edge effects are indeed observed as in eq S1, given in the Supporting Information, which is the equivalent of eq 5 valid for any tip-size, predicting the occurrence of a peak in the tip current approach curve.

(37) (a) Imabayashi, S.-I.; Hobara, D.; Kakiuchi, T. *Langmuir* **2001**, *17*, 2560−2563. (b) Stranick S. J.; Parikh, A. N.; Allara, D. L.; Weiss, P. S. *J. Phys. Chem.* **1994**, *98*, 11136−11142.

(38) (a) Subramanian, G.; Williams, D. R. M.; Pincus, P. A. *Europhys. Lett.* **1995**, *29*, 285−290. (b) Milchev, A.; Yamakov, V.; Binder, K. *Europhys. Lett.* **1995**, *47*, 675−680. (c) Ennis, J.; Sevick, E. M.; Williams D. R. M. *Phys. Rev. E* **1999**, *60*, 6906−6918. (d) Klushin, L. I.; Skvorstov, A. M.; Leermarkers, F. A. M. *Phys. Rev. E* **2004**, *69*, 061101, 1−15.

(39) Williams, D. R. M.; MacKintosh, F. C. *J. Phys. II* **1995**, *5*, 1407−1417.